IEEE Access
Multidisciplinary ⋮ Rapid Review ⋮ Open Access Journal

Received October 7, 2016, accepted October 16, 2016, date of publication January 2, 2017, date of current version February 25, 2017.

Digital Object Identifier 10.1109/ACCESS.2016.2636224

Robust Synchronous Control of Multi-Motor Integrated With Artificial Potential Field and Sliding Mode Variable Structure

CHANGFAN ZHANG[1], MANGANG NIU[1], JING HE[1,2], KAIHUI ZHAO[1], HAN WU[1], AND MIAOYING ZHANG[1]

[1]College of Electrical and Information Engineering, Hunan University of Technology, Zhuzhou 412007, China
[2]College of Mechatronics Engineering and Automation, National University of Defense Technology, Changsha 410000, China

Corresponding author: Jing He (hejing@263.net)

This work was supported in part by the Natural Science Foundation of China under Grant 61273157 and Grant 61473117, in part by the Hunan Provincial Natural Science Foundation of China under Grant 2016JJ5007, and in part by the Scientific Research Fund of the Hunan Provincial Education Department under Grant 16A058.

ABSTRACT This paper aims to study the issue of robust synchronous control of multi-motor. A scheme of synchronous motion based on the artificial potential field is proposed. In this scheme, a model of artificial potential field is constructed and by employing the methods for the flocking control and the sliding mode variable structure, the synchronous control is designed for the multi-motor system. Moreover, by using the Lyapunov method and the graph theory, the stability conditions of the controlled system and further the necessary conditions of multi-motor synchronous control are obtained. It shows that, under such designed control scheme, the robustness with respect to the variations of parameters and the synchronous performance of a multi-motor system can be improved. Finally, the simulation and experimental results illustrate the effectiveness of the proposed method.

INDEX TERMS System of multi-motor, synchronous control, flocking control, artificial field, sliding mode variable.

I. INTRODUCTION

Multi-agent coordination control has prospects of wide application and is important in industrial manufacturing. Researchers have conducted extensive studies in recent years to apply multi-agent coordination control in multi-robot, aircraft, and underwater vehicle fields, and the main research methods include consensus [1], [2] and formation [3], [4], containment [5]–[7], and flocking control [8], [9].

Synchronization is one of the most basic problems of multi-agent coordination control [10]. Khatib *et al.* [11] first proposed a strategy for flocking synchronous control based on an artificial potential field. The method has been applied successfully to multi-robot synchronous control. The basic idea of the strategy is to consider motion of the robot in the environment as motion in a virtual artificial stress field. It has been applied extensively in real-time obstacle avoidance and smooth trajectory control. Nakazawa *et al.* [12] designed an artificial potential field controller to maintain synchronous robot-human motion in a dynamic environment. Zhang *et al.* [13] solved the problem of a local minimum in robot motion by using a genetic algorithm to optimize artificial potential field parameters. Xie *et al.* [14] researched the application of synchronous control in an artificial potential field in the matching of biological cells.

Synchronization is also a core problem in multi-motor motion [15], [16]. Synchronizing drive control for multi-motors has been applied in various fields, such as paper machines, printing presses, textile machines, numerical control machines, and even in high-power, high-speed railway traction systems. The main traditional synchronous control for multi-motors is uncoupling and coupling control. Uncoupling control includes mainly master-slave and electronic virtual line-shafting control. Master-slave control can be realized easily because of its simple structure. However, it has weak robustness. Electronic virtual line shafting control increases feedback of the auxiliary shaft torque, and enhances synchronous performance [17]. Coupling control includes the cross-coupling synchronous control strategy proposed by Koren, and the relative coupling synchronous structure

proposed by Perez-Pinal [18]. Synchronous performance can be better realized, and the control algorithm is complex.

However, two problems require further research in synchronous control. The first is to build a mathematical model of the system. Existing literature considers the actual system as the point [19], that is, a simple integrator acts as the research object without considering the actual dynamic equation. However, no such simplified model exists in practical engineering. The second problem is robust flocking control, that is, how to consider parameter variations, external disturbances, and some other factors in designing the synchronous controller. Some scholars have researched only one of the problems. For example, a bank of observers are designed to study the state observation and unknown input identification problems with high-order sliding mode techniques [20], and a finite-time distributed consensus algorithm based on the sliding mode control is designed and the tracking time is estimated analytically [21]. Therefore, based on the construction of an actual system mathematical model, a robust synchronous controller of the multi-motor that integrates the artificial potential field with sliding mode variable structure is proposed for the parameter variation that exists in the model.

The paper is organized as follows. In section 2, a topological structure of the multi-motor is described. Section 3 proposes a multi-motor controller for the artificial potential field. Section 4 designs a multi-motor synchronous controller that integrates the artificial potential field with the sliding mode variable structure. Section 5 analyzes the simulation and experiment, and then summarize and recommend future research work in section 6.

II. TOPOLOGICAL STRUCTURE OF MULTI-MOTOR

Graph theory is used to describe the network topological structure [22], [23] of information transfer among the multi-agent in this paper. A flocking topological structure diagram based on a leader-follower multi-motor is designed to describe the relationship between each motor. Four practical motors are used as an example. A flocking topological structure diagram of multi-motor D_1 is given in Figure 1, where black circle represents (Leader Motor) M_0, white circles represent four Follower Motors $M_i(i = 1, 2, 3, 4)$, respectively. Dotted arrows represent relationship between each follower motor and leader motor, four follower motors running under the control of M_0.

Definition 1 [24]: A weighted directed graph D refers to an ordered triple $(V(D), H(D), W_D)$. $V(D) = \{v_1, v_2, \ldots, v_n\}$ is a nonempty set of nodes, which is termed the set of tops of D. The tops donate each motor agent. $H(D) = \{(v_i, v_j) \,|\, v_i, v_j \in V(D)\}$ is the set of edges of D. (v_i, v_j) is used to represent the connection of agent motor i and j. W_D is the weight of (v_i, v_j), and represents the interaction function between the agent motors i and j.

Definition 2 [24]: Adjacency matrix $A(D) = (a_{ij})_{n\times n}$, where a_{ij} is factor weight that agent motor v_i affects v_j. v_i is the starting point, v_j is the end, where $a_{ij} = 1$, otherwise

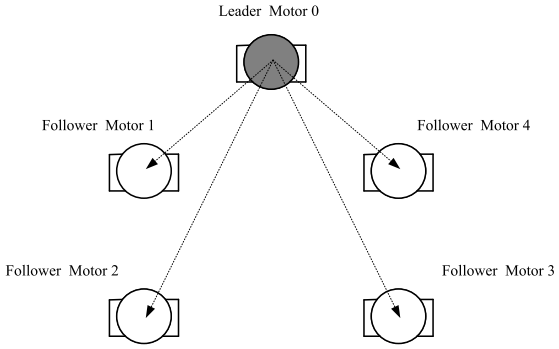

FIGURE 1. A flocking topological structure diagram of multi-motor D_1.

$a_{ij} = 0$. Incidence matrix $M(D) = (m_{ij})_{n\times m}$, if v_i is the start point of edge (v_i, v_j), $m_{ij} = 1$, if v_j is the end point of edge (v_i, v_j), $m_{ij} = -1$, otherwise $m_{ij} = 0$. Matrix $L(D) = M(D)M(D)^T$ is the *Laplacian* matrix of D. It presents most of features of Figure D, when D connected, $L(D)$ is positive semidefinite.

Definition 3: Angular position of leader motor is $\theta_0 = f(t)$, where $f(t)$ is the set value of angular position, real-time angular position of each follower motor is $\theta = [\theta_1\ \theta_2\ \ldots\ \theta_{n-1}]^T$. The actual angular position synchronous matrix is $D = \{D_{ij}\}_{n\times n}$, where $D_{ij} = \theta_i - \theta_j$ and $D_{ij} = 0, j = i$.

Through Definition 1 in the flocking topological structure diagram of multi-motor which is shown in Fig.1,$V(D_1) = \{v_{m0}, v_{m1}, v_{m2}, v_{m3}, v_{m4}\}$ presents five agent motors, edges (v_{m0}, v_{m1}), (v_{m0}, v_{m2}), (v_{m0}, v_{m3}) and (v_{m0}, v_{m4}) present the relationship of M_0 and M_i and effect is one-way, where M_0 leads M_i to move. We can obtain $A(D_1)$, $M(D_1)$ and $L(D_1)$ by combining Definition 2.

Adjacency matrix

$$A(D_1) = \begin{bmatrix} 0 & 0 & 0 & 0 & 0 \\ 1 & 0 & 0 & 0 & 0 \\ 1 & 0 & 0 & 0 & 0 \\ 1 & 0 & 0 & 0 & 0 \\ 1 & 0 & 0 & 0 & 0 \end{bmatrix}. \tag{1}$$

Incidence matrix

$$M(D_1) = \begin{bmatrix} 1 & 1 & 1 & 1 \\ -1 & 0 & 0 & 0 \\ 0 & -1 & 0 & 0 \\ 0 & 0 & -1 & 0 \\ 0 & 0 & 0 & -1 \end{bmatrix}. \tag{2}$$

Laplacian matrix

$$L(D_1) = \begin{bmatrix} 4 & -1 & -1 & -1 & -1 \\ -1 & 1 & 0 & 0 & 0 \\ -1 & 0 & 1 & 0 & 0 \\ -1 & 0 & 0 & 1 & 0 \\ -1 & 0 & 0 & 0 & 1 \end{bmatrix}, \tag{3}$$

$L(D_1)$ is positive semidefinite apparently.

Combining Figure 1 and Definition 3, we can get the actual angular position synchronous matrix D_1.

$$D_1 = \begin{bmatrix} 0 & \theta_0-\theta_1 & \theta_0-\theta_2 & \theta_0-\theta_3 & \theta_0-\theta_4 \\ \theta_1-\theta_0 & 0 & \theta_1-\theta_2 & \theta_1-\theta_3 & \theta_1-\theta_4 \\ \theta_2-\theta_0 & \theta_2-\theta_1 & 0 & \theta_2-\theta_3 & \theta_2-\theta_4 \\ \theta_3-\theta_0 & \theta_3-\theta_1 & \theta_3-\theta_2 & 0 & \theta_3-\theta_4 \\ \theta_4-\theta_{01} & \theta_4-\theta_1 & \theta_4-\theta_{21} & \theta_4-\theta_3 & 0 \end{bmatrix}. \tag{4}$$

Synchronous error matrix of multi-motor

$$E = (A(D_1) \circ D_1)1_{n\times 1}, \tag{5}$$

where '$\circ$' is product of Hadamard matrix, $1_{n\times 1} = (11\ldots1)^{\mathrm{T}}_{1\times n}$.

From Eq.(1), (4), (5), we can get synchronous error matrix E which is shown in Figure.1

$$E = \begin{bmatrix} 0 & 0 & 0 & 0 & 0 \\ \theta_1-\theta_0 & 0 & 0 & 0 & 0 \\ \theta_2-\theta_0 & 0 & 0 & 0 & 0 \\ \theta_3-\theta_0 & 0 & 0 & 0 & 0 \\ \theta_4-\theta_0 & 0 & 0 & 0 & 0 \end{bmatrix} \begin{bmatrix} 1 \\ 1 \\ 1 \\ 1 \\ 1 \end{bmatrix} = \begin{bmatrix} 0 \\ \theta_1-\theta_0 \\ \theta_2-\theta_0 \\ \theta_3-\theta_0 \\ \theta_4-\theta_0 \end{bmatrix}. \tag{6}$$

Form the above equation, we can see that if topological structure of multi-motor stays running synchronously, the synchronization error matrix $E = 0$, that is, $\theta_0 = \theta_i$. We can consider the interaction function W_D among motors in the graph theory as the motor controller. The motor controller is designed to meet the requirement of $\theta_0 = \theta_i$. The controller is designed by a combination of artificial potential field function and sliding mode variable structure to achieve real-time synchronization of the motor angular.

III. SYNCHRONOUS CONTROL OF ARTIFICIAL POTENTIAL FIELD

We apply the traditional artificial potential field model of the robot proposed by Leonard and Fiorelli [23], to the multi-motor synchronous control. As shown in Figure 1, the multi-motor agent system is composed of four followers and one leader. Force of the motor is shown in the arrow in the figure, the force f is generated by artificial potential field and the potential field function is V_1. V_1 and f among motors are decided by e between leader and follower motor, where $e = e_{leader} - e_{follower}$.

Definition 4: Potential field function of motor agent is defined as follows

$$V_1 = \begin{cases} \frac{1}{2}ke^2 + \ln(e+d) + \frac{d}{e+d} & |e| < d \\ \gamma & |e| \geq d, \end{cases} \tag{7}$$

where k is positive gain factor, d is positive real number, presenting maximum scope of agent potential field. γ is any real number, presenting agent potential field is a fixed value beyond maximum scope.

Definition 5: Potential field force f of motor agent is defined as follows

$$f = \begin{cases} -\rho_2 & -d < e < -d_1 \\ ke + \frac{e}{(e+d)^2} & -d_1 \leq e < d \\ 0 & |e| \geq d. \end{cases} \tag{8}$$

Relationship between f and e is shown in Figure 2.

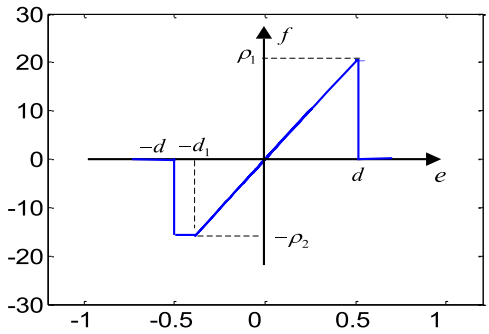

FIGURE 2. Relationship between f and e.

where ρ_1 and ρ_2 are the upper and lower bounds of f, respectively.

When $e \in (-d, d)$, Potential field force of motor,

$$\begin{cases} 0 < e < d & f > 0 \quad \textit{attractive force} \\ e = 0 & f = 0 \quad \textit{equilibrium point} \\ -d < e < 0 & f < 0 \quad \textit{repulsive force}. \end{cases} \tag{9}$$

From Figure 2 and Eq. (9), when $e = 0, f = 0$, which is the ideal equilibrium point, the leader and follower motors maintain synchronous running. When $0 < e < d, f > 0$, the potential field force behaves as an attractive force, that is, the leader motor attracts the follower motors. The physical result is an acceleration of the follower motors to synchronize with the leader motor. When $-d < e < 0, f < 0$, the potential field force behaves as a repulsive force, and the leader motor repels the follower motors. The physical result is a deceleration of the follower motors to synchronize with the leader motor.

Under synchronous control for the multi-motor with artificial potential field, if the motor parameters vary, the multi-motor controlled by the individual artificial potential field shows the phenomenon of chattering with large amplitude, and the follower motors cannot synchronize with the leader motor. Considering that the sliding mode variable structure control has a strong robustness, which does not change with system parameters and disturbance, if sliding mode variable structure control is added to the artificial potential field, real-time synchronous cooperation performance among the multi-motor will be improved effectively.

IV. SYNCHRONOUS CONTROL OF MULTI-MOTOR BY COMBINING ARTIFICIAL POTENTIAL FIELD WITH SLIDING MODE VARIABLE STRUCTURE

A. CONTROLLED OBJECT MODEL

A direct current motor is chosen as the agent, according to the equation for voltage and torque balance of the motor:

$$\begin{cases} U = Ri + L\dfrac{di}{dt} + E \\ E = c_e\omega \\ T_e - T_L = J\dfrac{d\omega}{dt} \\ T_e = k_m i, \end{cases} \tag{10}$$

where U is voltage of armature, R is the total resistance of armature circuit, L is inductance of armature winding, ω is speed of DC motor, i is armature current of motor, E is induction electromotive force of armature, c_e is voltage feedback coefficient, J is rotational inertia, k_m is electromagnetic torque coefficient, T_L is load torque, T_e is electromagnetic torque.

Under synchronous control for the multi-motor, we design a synchronous controller for the ith motor. States x_{1i} and x_{2i} are the angle and speed of motor i, respectively, where $x_{1i} = \theta_i$, $x_{2i} = \omega_i$. x_{1i} and x_{2i} are regarded as bounded variations in practical project.

From Eq. (10), the system state can be described by the equation

$$\begin{cases} \dot{x}_{1i}{=}x_{2i} \\ \dot{x}_{2i}{=}-a_i x_{2i}{+}b_i u_i, \end{cases} \tag{11}$$

where $a_i = \frac{k_{mi}c_{ei}}{J_i R_i}$, $b_i = k_{ui}\frac{k_{mi}}{J_i R_i}$, $a_i > 0, b_i > 0$.

When system parameter changes, the system parameters a_i, b_i are variable and respectively written as

$$\begin{cases} a_i = \bar{a}_i + \Delta a_i \\ b_i = \bar{b}_i + \Delta b_i, \end{cases} \tag{12}$$

where $\bar{a}_i$, $\bar{b}_i$ are nominal value of parameters, Δa_i, Δb_i are variation of corresponding parameters. Assuming that variation is bounded, that is $|\Delta a_i| < \delta_{1i}$, $|\Delta b_i| < \delta_{2i}$, and δ_{1i}, δ_{2i} is bounded positive number.

The synchronous control strategy graph of a multi-motor that integrates the artificial potential field with a sliding mode variable structure is constructed as shown in Figure 3.

Assuming that angular error is e_{1i}, $e_{1i} = x_d - x_{1i}$, speed error e_{2i}, $e_{2i} = \dot{x}_d - x_{2i}$, angular of leader motor is x_d, $x_d = \theta_0 = \theta_d$, speed of leader motor is $\dot{x}_d$, and x_d, $\dot{x}_d$, $\ddot{x}_d$ are bounded.

The linear sliding mode surface is selected as

$$s_i = c_i e_{1i} + e_{2i}, \tag{13}$$

where c_i is a being designed positive slope of the sliding mode surface.

Theorem 1: For the controlled object described by Eqs. (11) and (12), the multi-motor synchronous controller can be designed as the following controller, which combines the artificial potential field and sliding mode variable structure.

$$u_i = u_{1i} + u_{2i}, \tag{14}$$

where $u_{1i} = k_{1i}e_{1i} + \frac{e_{1i}}{(e_{1i}+d)^2}$ is artificial potential field control. $u_{2i} = k_{2i}sgn(s_i)$ is sliding mode variable structure control, $sgn(s_i)$ is a signum function, $i = 1, 2...n$.

If control coefficients $k_{1i} > 0$, k_{2i} is sufficiently large, the e_{1i}, e_{2i} are uniform convergence.

Proof: Choosing Lyapunov function

$$V_i = \frac{1}{2}s_i^2. \tag{15}$$

From Eqs. (11)-(15), we obtain that,

$$\begin{aligned} \dot{V}_i &= s_i\dot{s}_i = s_i[c_i e_{2i} + \ddot{x}_d + a_i x_{2i} - b_i u_{1i} - \Delta b_i u_{2i} - \bar{b}_i u_{2i}] \\ &= s_i[\ddot{x}_d + a_i x_{2i} - b_i u_{1i} - \Delta b_i u_{2i} + c_i e_{2i} - \bar{b}_i k_{2i} sgn(s_i)] \\ &\le |s_i|\,[|\Delta f_i| - \bar{b}_i k_{2i}], \end{aligned} \tag{16}$$

where

$$\Delta f_i = \ddot{x}_d + a_i x_{2i} - b_i u_{1i} - \Delta b_i u_{2i} + c_i e_{2i}. \tag{17}$$

From the above analysis and assumptions, all variables in Δf_i are bounded, that is $|\Delta f_i| < F_i$, and F_i is bounded positive number.

Therefore, if we choose a positive constant k_{2i}, such that

$$k_{2i} \ge \frac{1}{\bar{b}_i}(F_i + \eta_i), \tag{18}$$

where η_i is a positive constant.

Then, it follows

$$\dot{V}_i \le -\eta_i\,|s_i|\,, \tag{19}$$

which implies that $\dot{V}_i$ is negative definite. A sliding mode motion can be driven to the sliding mode surface in finite time. As long as the sliding mode motion reaches the sliding mode surface, based on the equivalence principle of sliding mode control [25], [26], we obtain

$$s_i = \dot{s}_i = 0. \tag{20}$$

It follows from (13) and (20) that

$$e_{1i}(t) = e_{1i}(0)e^{-c_i t},\ e_{2i}(t) = e_{2i}(0)e^{-c_i t}. \tag{21}$$

From (21) we can further obtain that

$$\lim_{t\to\infty} e_{1i}(t) = 0,\ \lim_{t\to\infty} e_{2i}(t) = 0. \tag{22}$$

This completes the proof. □

According to the topological structure graph of a multi-motor in Figure 1, the multi-motor synchronous control strategy graph is constructed in Figure 3. The controller is designed as u_i in Theorem 1, then $e_{1i} = 0$, namely $\theta_0 = \theta_i (i = 1, 2, 3, 4)$, is obtained. Consequently, the synchronization error matrix $E = 0$ of the angular position is obtained.

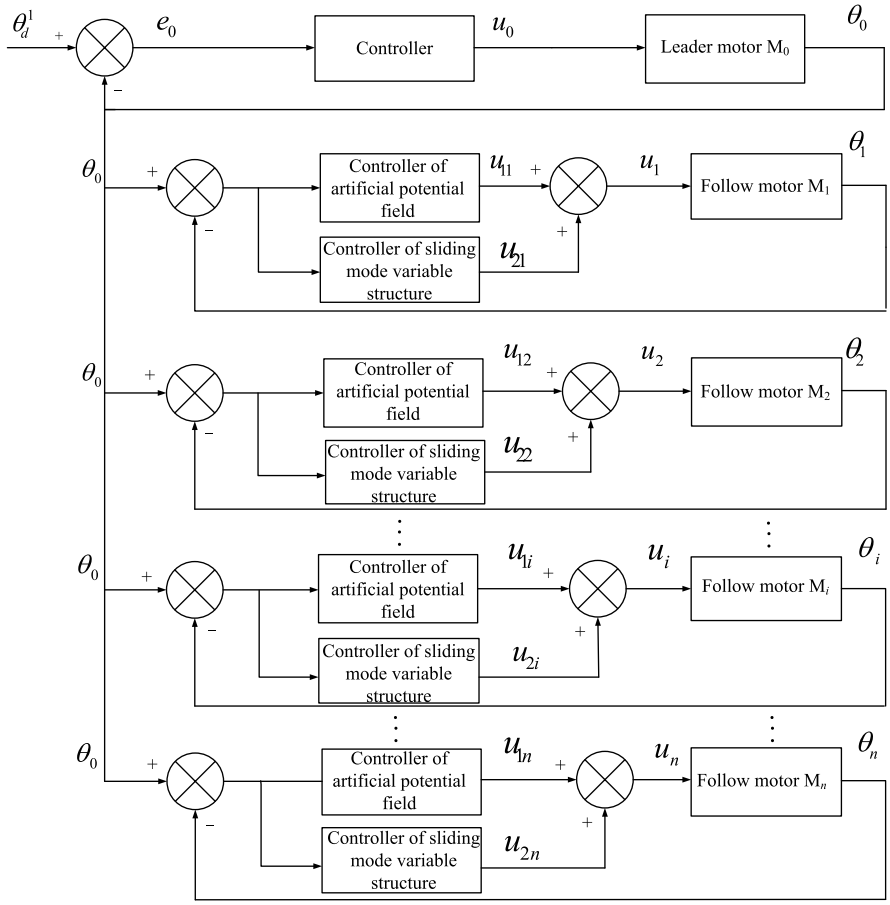

FIGURE 3. The synchronous control strategy graph of a multi-motor that integrates the artificial potential field with a sliding mode variable structure.

TABLE 1. Five motors nominal value parameters.

Motor number	$R(\Omega)$	k_m	C_e	$J(kg{\cdot}m^2)$	k_u
0	7.77	6	1.2	0.6	11
1	7.77	6	1.2	0.6	11
2	6	6.5	2	1.2	16.6
3	6.5	7	2	1.07	15.9
4	7	5.5	2	1	16

V. THE SIMULATION AND EXPERIMENTAL ANALYSIS

A. THE SIMULATION ANALYSIS

Simulation research is conducted on the established model and controller using simulation software MATLAB/Simulink. M_0 and M_1, M_2, M_3, M_4 are the leader and follower motors, respectively. The given angle of M_0 is $\theta_0 = \sin(t)$rad. Parameter settings of five direct current servo motors are given in Table 1.

1) SIMULATION EXPERIMENT 1

When parameters of motor are fixed, we use artificial potential field controller.

To verify the validity of the artificial potential field algorithm shown in Eq. (8), simulation analysis is conducted for the multi-motor flocking topological structure graph in Figure 1 for invariable motor parameters. The initial values of angular position of the follower motor M_1, M_2, M_3, M_4 are -0.1rad, -0.2rad, -0.25rad, -0.4rad, respectively. When the motor parameters are invariable, the tracking diagram of the angular position of M_1 is shown in Figure 4. M_1 can match M_0 within 2s. The tracking error in Figure 5 shows that the tracking error of the single motor gradually converges to zero.

The above simulation is a single motor to follow the leader motor. The tracking and synchronous error graphs

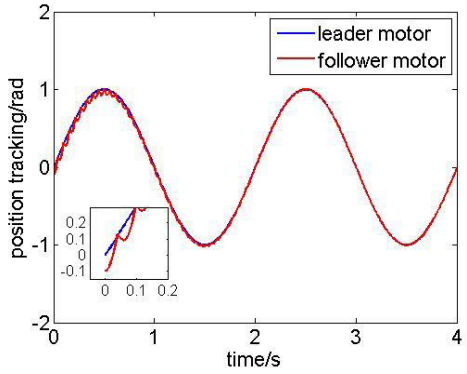

FIGURE 4. Position tracking of M_1.

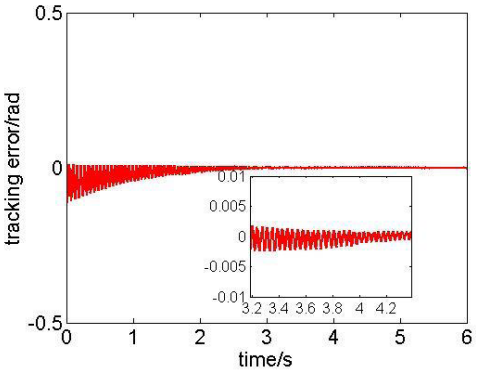

FIGURE 5. Tracking error of M_1.

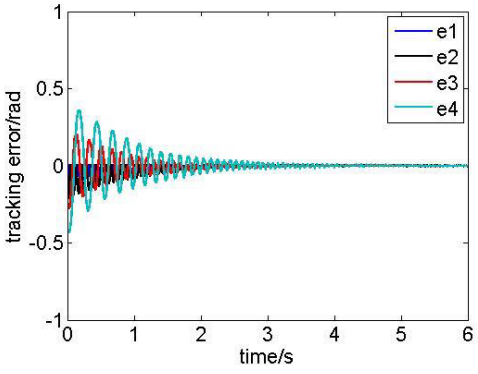

FIGURE 6. Tracking error based on artificial potential field.

of the entire motor will be presented to analyze the entire synchronous performance of the multi-motor. The angular error graph of four follower motors is shown in Figure 6, where $e_i = \theta_i - \theta_d$. A synchronous error of the motor angle is shown in Figure 7, and the synchronous error is defined as $E_i = \theta_i - \theta_{i+1} (i = 1, 2, \ldots, n)$. When $\theta_i = \theta_{i+1}$, $E_i = 0$, and complete synchronization between each motor is achieved. The simulation graph shows that each motor can achieve synchronization in a certain period of time under artificial potential field control, while the synchronous time is relatively long.

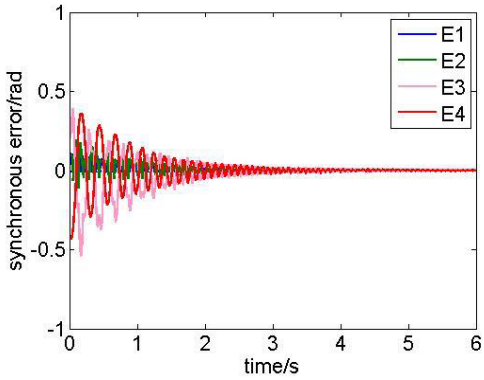

FIGURE 7. Synchronous error based on artificial potential field.

2) SIMULATION EXPERIMENT 2

When parameters of motor are variable, we use the controller that integrates the artificial potential field with the sliding mode variable structure designed in this paper.

Eq. (14) is the control algorithm that integrates the artificial potential field with the sliding mode variable structure. Eq. (8) is the artificial potential field algorithm. If we consider that the motor parameters are variable, nominal parameter values are listed in Table 1, and the variables $\Delta a_i = \sin(t)$, $\Delta b_i = 10 \sin(t)$. Firstly, we analyze the tracking performance of the single follower motor M_1. The performance and tracking error of the motor under control of a combination of artificial potential field with sliding mode variable structure and that under control of the artificial potential field are shown in Figs. 8 and 9. The former motor in Figure 8 can track the leader motor within 0.5s by using three times less time than that in Figure 9 and the tracking error of the single motor converges to zero, whereas the motor under the artificial potential field requires 2s to track the leader motor.

We then analyze the synchronous coordination of the whole motor. When the motor parameters are variable, the tracking error graph of angular of the entire motor based on a synchronous controller that combines the artificial potential field and sliding mode variable structure is shown in Figure 10(a). The tracking error graph of the multi-motor angular under control of the artificial potential field is shown in Figure 10(b). A comparison of two simulation results shows that the former converges to zero at 0.3s, and has almost no chattering. The latter also converges to zero at 3s, however, chattering occurs. Therefore, the entire tracking effect for the controller that integrates the artificial potential field with the sliding mode variable structure is better than that of the separate artificial potential field.

Figure 11(a) shows the entire synchronous error graph based on control that combines the artificial potential field and sliding mode variable structure. The multi-motor synchronous error graph under control of the artificial potential field is shown in Figure 11(b). The synchronous error under control of the artificial potential field and the sliding mode

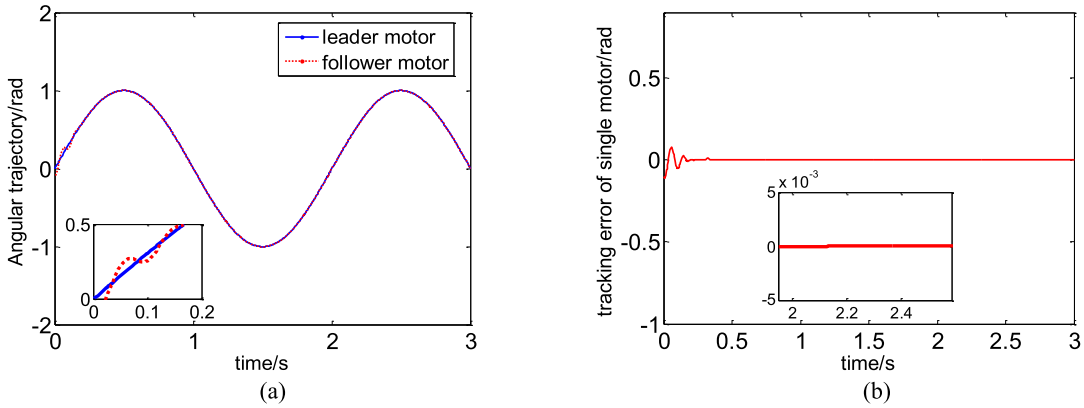

FIGURE 8. Tracking graph of M_1 based on artificial potential field with sliding mode variable structure.

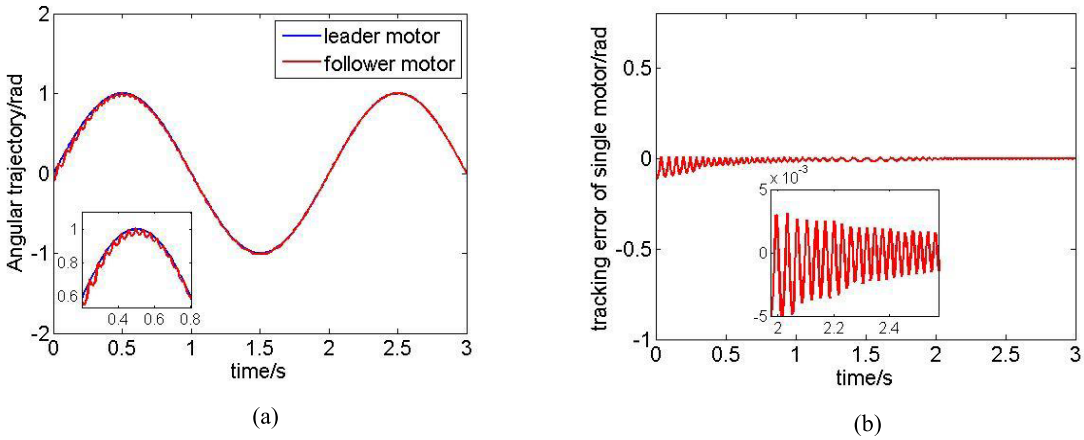

FIGURE 9. Tracking graph of M_1 based on artificial potential field.

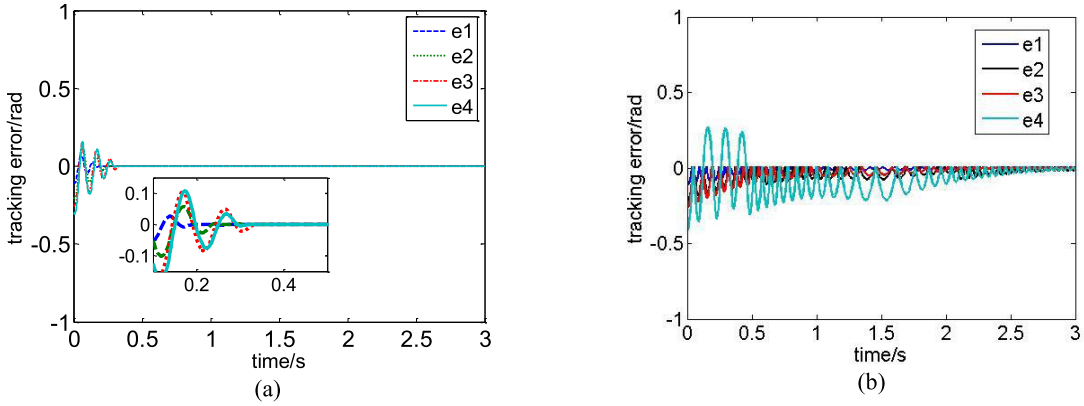

FIGURE 10. Comparison of tracking error. (a) Tracking error based on artificial potential field with sliding mode variable structure. (b) Tracking error based on artificial potential field.

variable structure completes synchronization within 0.4s, and exhibits almost no chattering later, when the motor parameters are variable. The synchronous error under control of the separate artificial potential field fluctuates up or down by at 2.5s, and chattering occurs later. Moreover, the precision of the synchronous error is lower than the former. The synchronous error $J_1 = 0.25 \int_0^\infty \sum_{i=1}^{4} |E_i| dt = 0.009$ based on control that combines the artificial potential field and sliding mode variable structure. The synchronous error is $J_2 = 0.25 \int_0^\infty \sum_{i=1}^{4} |E_i| dt = 0.075$ under control of the arti-

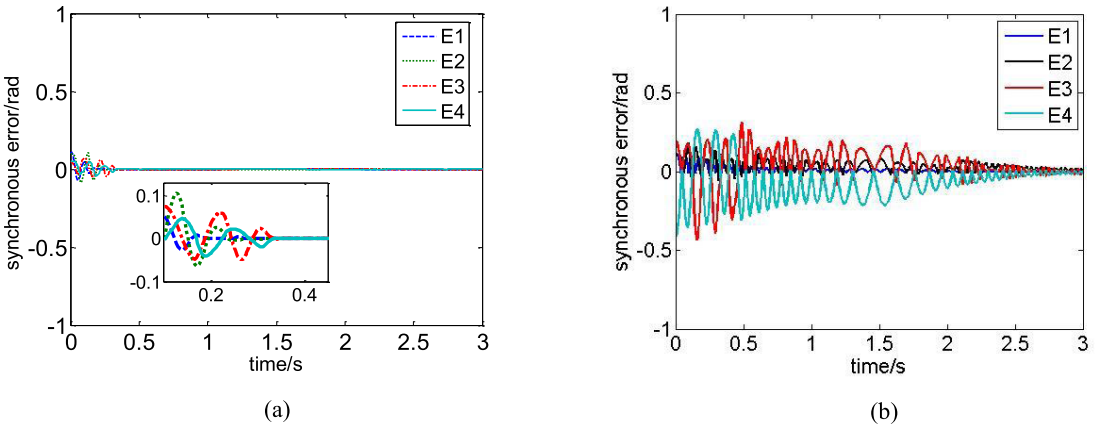

FIGURE 11. Comparison of synchronous error. (a) Synchronous error based on artificial potential field with sliding mode variable structure. (b) Synchronous error based on artificial potential field.

ficial potential field. Therefore, the controller that integrates the artificial potential field with the sliding mode variable structure can cope with a variation in parameters in multi-motor synchronization more effectively.

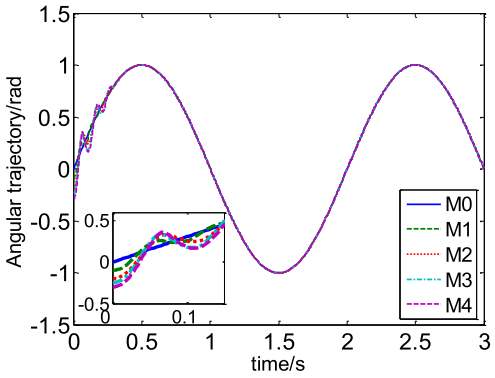

FIGURE 12. Position tracking of M_i ($i = 1, 2, 3, 4$) based on artificial potential field with sliding mode variable structure.

Figure 12 is simulation result of the dynamic response of the position tracking between the actual motor (follower motor) Mi ($_i = 1, 2, 3, 4$) and reference motor(leader motor) M_0 based on artificial potential field with sliding mode variable structure.

The above simulation results indicate that the designed controller of the artificial potential field of the motor can maintain synchronous running of the multi-motor, when the parameter are invariable. However, when the parameters vary with time, the effects of tracking and synchronous errors are both relatively poor. The controller that integrates the artificial potential field with the sliding mode variable structure can overcome the influence from a variation in parameters. It possesses excellent tracking performance for the single controller, and can also complete rapid synchronous requirements of real-time angular of multi-motors with small chattering amplitude, high synchronous precision and rapid convergence rate.

B. EXPERIMENTAL ANALYSIS

The semi-physical simulation platform RT-Lab is used. RT-Lab OP5600 and the controller TMS320F2812 are used for the experimental simulation with the following experimental process. Compiled code is downloaded from the model of the motor system, and transferred to OP5600. Then code C that is downloaded from the designed controller model is transferred to TMS320F2812 to run. This achieves the hardware in the loop of the controller in the semi-physical simulation [16]. The sampling period is set at 5 μs. The RT-Lab platform is shown in Figure 13.

FIGURE 13. RT-Lab experiment setup.

Parameters and condition of the motor selected in the experiment are the same as those of section 5.1. The controller of the artificial potential field in Eq. (8) is used in the experiment of multi-motor synchronous control. A graph of the angular position of the four follower motors is shown

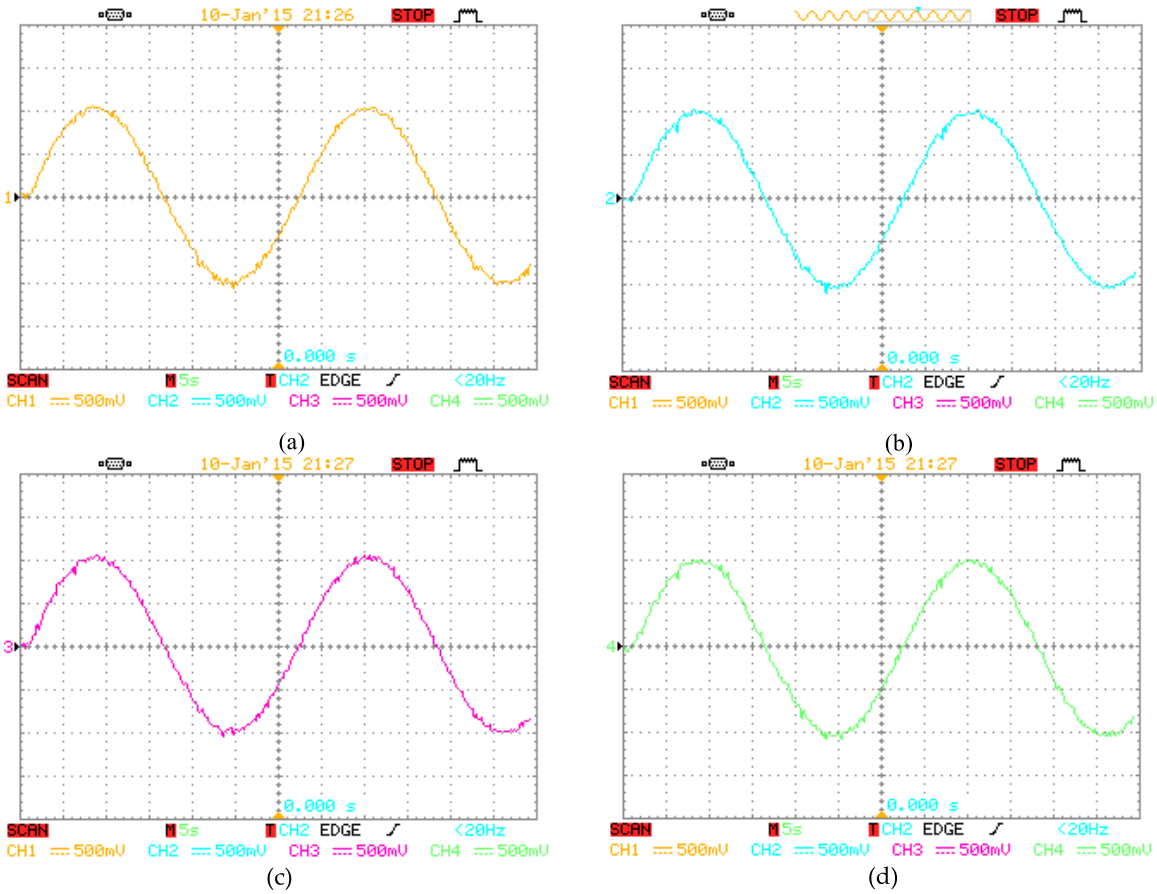

FIGURE 14. Angular position of the four follower motors based on RT-Lab(θ: 0.5rad /case).

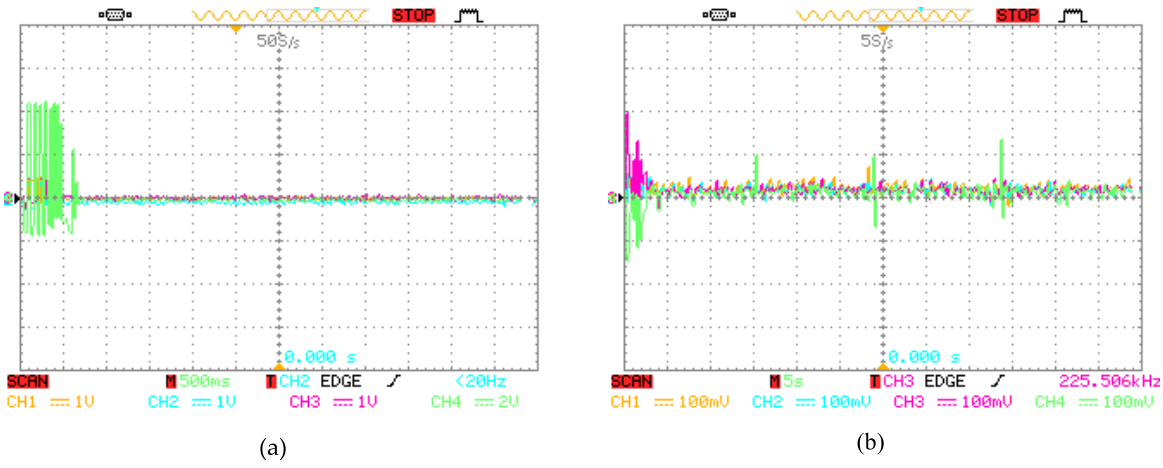

FIGURE 15. Angular tracking and synchronous error obtained by controller of artificial potential field based on RT-Lab. (a) Tracking error(e:0.2rad/case). (b) Synchronous error(E: 0.25rad/case).

in Figure 14 and the four motors can all follow the leader motor.

For the experiment of synchronous motion of the multi-motor with variable parameters, the controller of the artificial potential field in Eq. (8) and the controller that integrates the artificial potential field with the sliding mode variable structure in Eq. (14) are applied for comparison. The experimental results of the former are shown in Figure 15, with the tracking and synchronous error graphs shown in Figs. 15 (a) and 15 (b), respectively. Results from the latter are shown in Figure 16, where the tracking and synchronous error graphs are shown in Figs. 16 (a) and 16 (b), respectively.

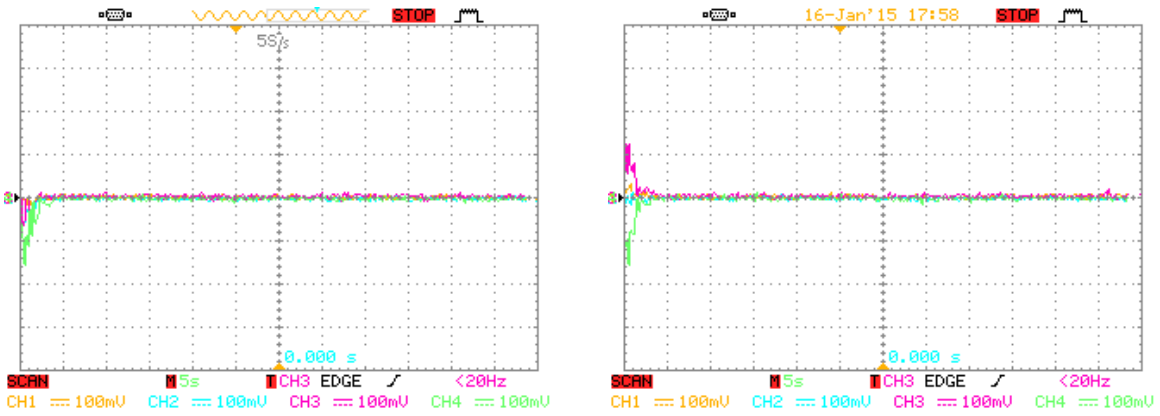

(a) (b)

FIGURE 16. Angular tracking and synchronous error obtained by controller that integrates the artificial potential field with the sliding mode variable structure based on RT-Lab. (a) Tracking error(e:0.2rad/case). (b) Synchronous error(E: 0.25rad/case).

A comparison of the tracking and synchronous error graphs shows that the results based on the simulation platform RT-Lab are the same as those from simulation analysis MATLAB. When the motor parameters are variable, the speed of the following and synchronous errors of the multi-motors under the control of the artificial potential field and the sliding mode variable structure converges to zero faster than that of the controller of the separate artificial potential field. In addition, the track is relatively smooth.

VI. CONCLUSION

The paper aims to address two core problems: identifying a new synchronous strategy for multi-motors and increasing the system synchronism and robustness. The synchronous control strategy for a multi-motor system that integrates an artificial potential field with sliding mode variable structure is proposed. Graph theory is used to analyze the multi-motor topological structure. Then, an artificial field model which combines flocking control is constructed. Synchronous operation of each follower motor with a leader motor is realized by interaction of the attractive and repulsive forces of the leader motor. In engineering practice, motor parameters are variable, whereas the sliding mode of the sliding mode variable structure can be designed affected by parameters of system and disturbance. To increase the robustness for multi-motor synchronization, a multi-motor synchronous controller that integrates an artificial potential field with a sliding mode variable structure is designed. The controller stability is proved by the Lyapunov method. The tracking and synchronous performance of the controller that integrates the artificial potential field with the sliding mode variable structure is improved and strong robustness over the artificial potential field controller is illustrated by simulation results. The effectiveness of the controller is further verified using experimental platform RT-Lab.

AUTHOR CONTRIBUTIONS

Changfan Zhang, Mangang Niu and Jing He designed the overall algorithms and the simulations. Mangang Niu, Kaihui Zhao, Han Wu, and Miaoying Zhang designed the experiments and performed the simulations and experiments. Changfan Zhang and Mangang Niu wrote the manuscript.

CONFLICTS OF INTEREST

The authors declare no conflict of interest.

REFERENCES

[1] H. Su, M. Z. Q. Chen, and G. Chen, "Robust Semi-global coordinated tracking of linear multi-agent systems with input saturation," *Int. J. Robust Nonlinear Control*, vol. 25, no. 14, pp. 2375–2390, Sep. 2015.

[2] H. Su, M. Z. Q. Chen, X. Wang, and J. Lam, "Semiglobal observer-based leader-following consensus with input saturation," *IEEE Trans. Ind. Electron.*, vol. 61, no. 6, pp. 2842–2850, Jun. 2014.

[3] H. Zhang, G. Feng, H. Yan, and Q. Chen, "Observer-based output feedback event-triggered control for consensus of multi-agent systems," *IEEE Trans. Ind. Electron.*, vol. 61, no. 9, pp. 4885–4894, Sep. 2014.

[4] Z. Wang and D. Gu, "Cooperative target tracking control of multiple robots," *IEEE Trans. Ind. Electron.*, vol. 59, no. 8, pp. 3232–3240, Aug. 2012.

[5] X. Dong, Q. Li, R. Wang, and Z. Ren, "Time-varying formation control for second-order swarm systems with switching directed topologies," *Inf. Sci.*, vol. 369, pp. 1–13, Nov. 2016.

[6] C. Xu, Y. Zheng, H. Su, Wang, and H. O. Wang, "Containment control for coupled harmonic oscillators with multiple leaders under directed topology," *Int. J. Control*, vol. 88, no. 2, pp. 248–255, 2015.

[7] C. Xu, Y. Zheng, H. Su, and H.-B. Zeng, "Containment for linear multi-agent systems with exogenous disturbances," *Neurocomputing*, vol. 160, pp. 206–212, Jul. 2015.

[8] H. Su, X. Wang, and Z. Lin, "Flocking of multi-agents with a virtual leader," *IEEE Trans. Autom. Control.*, vol. 54, no. 2, pp. 293–307, Feb. 2009.

[9] B. Fidan, V. Gazi, S. Zhai, N. Cen, and E. Karataş, "Single-view distance-estimation-based formation control of robotic swarms," *IEEE Trans. Ind. Electron.*, vol. 60, no. 12, pp. 5781–5791, Dec. 2013.

[10] A. Jevtić and Á. Gutiérrez, "Distributed bees algorithm parameters optimization for a cost efficient target allocation in swarms of robots," *Sensors*, vol. 11, no. 11, pp. 10880–10893, 2011.

[11] O. Khatib, "Real-time obstacle avoidance for manipulators and mobile robots," *Int. J. Robot. Res.*, vol. 5, no. 1, pp. 90–98, 1986.

[12] K. Nakazawa, K. Takahashi, and M. Kaneko, "Movement control of accompanying robot based on artificial potential field adapted to dynamic environments," *Elect. Eng. Jpn.*, vol. 192, no. 1, pp. 25–35, Jul. 2015.

[13] Q. Zhang, D. Chen, and T. Chen, "An obstacle avoidance method of soccer robot based on evolutionary artificial potential field," *Energy Procedia*, vol. 16, pp. 1792–1798, 2012.

[14] M. Y. Xie, Y. Wang, and D. Sun, "Optical manipulation of pairing biological cells using an artificial potential field based controller," in *Proc. 9th IEEE Int. Conf. Nano/Micro Eng. Molecular Syst. (NEMS)*, Waikiki Beach, HI, USA, Apr. 2014, pp. 544–548.
[15] A. Jimenez-Fernandez, G. Jimenez-Moreno, A. Linares-Barranco, M. J. Dominguez-Morales, R. Paz-Vicente, and A. Civit-Balcells, "A neuro-inspired spike-based PID motor controller for multi-motor robots with low cost FPGAs," *Sensors*, vol. 12, no. 4, pp. 3831–3856, 2012.
[16] S. Abourida, C. Dufour, J. Belanger, T. Yamada, and T. Arasawa, "Hardware-in-the-loop simulation of finite-element based motor drives with RT-LAB and JMAG," in *Proc. IEEE Int. Symp. Ind. Electron.*, Montreal, QC, Canada, Jul. 2006, pp. 2462–2466.
[17] R. G. Anderson, A. J. Meyer, M. A. Valenzuela, and R. D. Lorenz, "Web machine coordinated motion control via electronic line-shafting," *IEEE Trans. Ind. Appl.*, vol. 37, no. 1, pp. 247–254, Jan./Feb. 2001.
[18] F. J. Perez-Pinal, "Improvement of the electronic line-shafting," in *Proc. IEEE 35th Annu. Power Electron. Specialists Conf.*, Aachen, Germany, Jun. 2004, pp. 3260–3265.
[19] X. Y. Luo, F. Yang, S. B. Li, and X. P. Guan, "Generation of optimally persistent formation for multi-agent systems," *Acta Autom. Sinica*, vol. 40, no. 7, pp. 1311–1319, Jul. 2014.
[20] H. Ríos, J. Davila, and L. Fridman, "High-order sliding mode observers for nonlinear autonomous switched systems with unknown inputs," *J. Franklin Inst.*, vol. 349, no. 10, pp. 2975–3002, Dec. 2012.
[21] X. Xu and J. Wang, "Finite-time consensus tracking for second-order multiagent systems," *Asian J. Control*, vol. 15, no. 4, pp. 1246–1250, Jul. 2013.
[22] A. Jadbabaie, J. Lin, and A. S. Morse, "Coordination of groups of mobile autonomous agents using nearest neighbor rules," *IEEE Trans. Autom. Control*, vol. 48, no. 6, pp. 988–1001, Jun. 2003.
[23] W. Ren and R. W. Beard, "Consensus seeking in multiagent systems under dynamically changing interaction topologies," *IEEE Trans. Autom. Control*, vol. 50, no. 5, pp. 655–661, May 2005.
[24] D. V. Dimarogonas and K. H. Johansson, "Stability analysis for multi-agent systems using the incidence matrix: quantized communication and formation control," *Automatica*, vol. 46, no. 4, pp. 695–700, Apr. 2010.
[25] N. E. Leonard and E. Fiorelli, "Virtual leaders, artificial potentials and coordinated control of groups," in *Proc. 40th IEEE Conf. Decision Control*, Orlando, FL, USA, Dec. 2001, pp. 2968–2973.
[26] U. Itkin, *Control Systems of Variable Structure*. New York, NY, USA: Wiley, 1976.

CHANGFAN ZHANG received his M.S. degree from Southwest Jiaotong University and his Ph.D. degree from Hunan University, China, in 1989 and 2001, respectively. He is currently a professor at College of Electrical and Information Engineering, Hunan University of Technology. His research interests include fault diagnosis on electric machines and industrial process control.

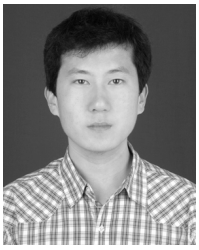

MANGANG NIU received his B.S. degree and his M.S. degree from Hunan University of Technology, China, in 2012 and 2015, respectively. He is currently an engineer in CRRC Zhuzhou Institute. His research interests include battery system design and application.

JING HE received her M.S. degree from Central South University of Forestry and Technology in 2002, and her Ph.D. degree from National University of Defense Technology, China, in 2009. She is currently a professor at the College of Electrical and Information Engineering, Hunan University of Technology. Her research interests include fault diagnosis on mechatronics and industrial process control.

KAIHUI ZHAO received his Ph.D. degree from Central South University, China in 2015. He is currently a associate professor at School of Electrical and Information Engineering, Hunan University of Technology, China. His research interests include fault diagnosis on electric machines.

HAN WU received her M.S. degree in power electronics and power transmission from Hunan University of Technology, Zhuzhou, China, in 2015. She is currently a Ph.D. candidate in control theory and control engineering from Huazhong University of Science and Technology, Wuhan, China. Her research interests include cooperation of multi-agent systems and complex networks.

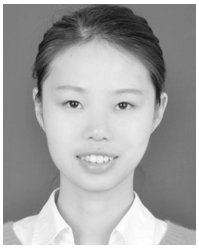

MIAOYING ZHANG received her M.S. degree from Hunan University of Technology, China, in 2015. She is currently a teacher at Hunan Railway Professional Technology College. Her research interests include power transmission technology and fault diagnosis.